

A First-Principles Thermodynamic Uncertainty Relation for Shortcuts to Adiabaticity

Guillermo Perna^{*1}, Federico Centrone^{†2}, and Esteban Calzetta^{‡3}

^{1,3}Universidad de Buenos Aires, Facultad de Ciencias Exactas y Naturales, Departamento de Física. Buenos Aires, Argentina, and CONICET - Universidad de Buenos Aires, Instituto de Física de Buenos Aires (IFIBA). Buenos Aires, Argentina

²ICFO-Institut de Ciències Fòniques, The Barcelona Institute of Science and Technology, Av. Carl Friedrich Gauss 3, 08860 Castelldefels (Barcelona), Spain.

March 13, 2026

Abstract

We study the fundamental limitations of implementing time-dependent Hamiltonian protocols when “time” is provided by a quantum clock rather than an external classical parameter. For a parametric harmonic oscillator controlled through a shortcut-to-adiabaticity (STA) schedule and coupled to a minimal clock degree of freedom, tracing out the clock yields an effective reduced dynamics that is a mixture of unitary Gaussian trajectories. Within a noise-dominated regime, we compute the energetic deviation from the target STA outcome and its fluctuations, together with the fidelity to the target evolution and the purity loss of the reduced state, for vacuum and coherent initial states. Combining these observables produces a thermodynamic-uncertainty-type tradeoff that links achievable precision to an irreducible loss of purity set by the clock precision and the protocol sensitivity.

1 Introduction

Time-dependent Hamiltonians are the standard language of quantum control, quantum thermodynamic strokes, and gate implementation: one prescribes a schedule $H(t)$ and computes the corresponding unitary $U = \mathcal{T} \exp \left[-\frac{i}{\hbar} \int_0^{t_f} dt H(t) \right]$. Within this framework, a large body of work has developed protocols that suppress nonadiabatic excitations and enable high-fidelity state preparation in finite time. A prominent example is the family of *shortcuts to adiabaticity* (STA), where suitably engineered drivings reproduce (or closely approximate) the outcome of an adiabatic process without requiring slow evolution [1, 2].

This standard control-theoretic picture treats t as an external classical parameter. However, if one insists on a first-principles description of a closed quantum world, the fundamental dynamics is generated by a time-independent Hamiltonian on a larger Hilbert space. In that setting, a time-dependent Hamiltonian for a subsystem can only emerge effectively: the subsystem must be coupled to additional degrees of freedom whose evolution is used as a time reference. This is not a merely interpretational point. Once a clock is included, the global evolution remains unitary, but the reduced dynamics of the controlled subsystem need not be unitary because the clock can become correlated with it. The operational question is then unavoidable:

What is the intrinsic decoherence and precision limit of a time-dependent unitary protocol when the only source of “time” is a quantum clock?

^{*}gperna@df.uba.ar

[†]Federico.Centrone@icfo.eu

[‡]calzetta@df.uba.ar

This perspective is central to relational approaches to time in quantum theory [3], where dynamics can be understood conditionally with respect to an internal time reference, and it also appears, in a different guise, in proposals where the *quantumness* of clocks leads to an effective loss of coherence for subsystems when the clock is ignored [4].

In an autonomous description, these effects do not rely on adding ad hoc classical noise or on continuously measuring the clock. Rather, they arise because a time reference is itself a quantum system whose degrees of freedom become entangled with the controlled dynamics when they generate the schedule and are subject to the uncertainty principle. From the reduced point of view in which the clock is discarded, this unavoidable entanglement manifests as a spread of effective “histories” for the control and hence as an effectively nonunitary map on the system. In other words, even in the absence of any environment, can the *implementation* of a time-programmed protocol generate mixedness and limit fidelity to the intended target, solely because timekeeping is quantum?

The present work pursues this question in a setting where both the control objective and the clock-induced limitation can be characterized analytically. We consider a parametric harmonic oscillator driven by a STA protocol and replace the externally prescribed time dependence by a fully autonomous system–clock model in which the oscillator frequency depends on a clock coordinate. This builds directly on Ref. [5], where an autonomous clock implementation of STA was introduced and it was shown that, even in the absence of any external environment, system–clock correlations generically deflect the evolution from the ideal STA trajectory and lead to a spread of outcomes once the clock is ignored.

Here we go beyond that analysis by reframing the effect as a limitation of *time-programmed quantum operations*: we treat the ideal STA evolution (obtained in the limit of a sharply defined clock trajectory) as a *target unitary/state-preparation task*, and we quantify (i) the degradation of the target (fidelity), (ii) the induced mixedness upon tracing out the clock (purity loss/irreversibility), and (iii) energetic deviations and fluctuations as complementary diagnostics of the same mechanism. Importantly, the resulting “noise” is not an extra stochastic ingredient added by hand: it is a compact parametrization of the unitary entangling dynamics between system and a quantum time reference, viewed from the reduced description in which the clock degrees of freedom are discarded.

STA provides a particularly clean benchmark for this purpose. In the ideal description with a perfectly classical time parameter, STA can be arranged so that deterministic nonadiabatic excitations vanish by construction. Any residual excitations, loss of fidelity, or loss of purity in our autonomous model can therefore be attributed to the quantumness of the time reference—rather than to an imperfect choice of schedule—thereby isolating what is truly *intrinsic to timekeeping*.

Methodologically, we start from the unitary dynamics of the combined system–clock and trace out the clock using a Feynman–Vernon influence functional [6, 7]. In the regime studied here, the clock induces an effectively stochastic modulation of the oscillator frequency: each realization corresponds to a unitary evolution of the oscillator, while decoherence arises only after averaging over realizations (equivalently, after discarding the clock). This provides a controlled and microscopic route from an autonomous Hamiltonian description to an operationally meaningful “error model” for time-dependent control.

Conceptually, we aim to connect this clock-induced mechanism to a tradeoff between *precision* and *irreversibility* for time-programmed protocols. Such tradeoffs resonate with broader discussions of the thermodynamic cost of timekeeping and the limitations of clocks [8, 9]. In our case, the relevant figures of merit are not extracted from an external bath or measurement record: they arise from unitary system–clock correlations alone.

The quantum nature of the “control knob” has long been recognized as a potential limitation for idealized time-dependent protocols: quantizing the control field (e.g. a laser mode) generically entangles it with the target and induces dephasing/errors when the control is discarded [10, 11, 12, 13], with error scalings tied to control resources [14, 15]. Complementary approaches model imperfect timekeeping as an uncertainty in the duration of an intended operation (random time) [16, 17], while recent work develops fully autonomous clock-driven dynamics in which a quantum clock generates the schedule without external time dependence [18, 19]. Our contribution lies at this intersection: we study a genuinely time-programmed

Hamiltonian protocol (STA for a parametric oscillator) implemented by a minimal quantum clock, derive the induced random-unitary description from first principles, and—building on the autonomous-STA framework of [5]—connect fidelity loss and purity loss to energetic deviations through a thermodynamic-uncertainty-type tradeoff, with analytic results in a controlled small-noise regime (including arbitrary Gaussian inputs).

The paper is organized as follows. In Sec. 2 we introduce the autonomous system–clock Hamiltonian and derive the reduced dynamics of the oscillator by tracing out the clock degrees of freedom. In Sec. 3 we analyze the unitary dynamics associated with a single clock trajectory and express the evolution in terms of symplectic maps and Bogoliubov coefficients. In Sec. 4 we define the relevant observables—energetic deviations, fidelity with respect to the target STA evolution, and purity loss—and evaluate their clock-averaged behavior in the small-noise regime. These quantities are then combined to establish a thermodynamic-uncertainty-type relation linking precision, energetic fluctuations, and irreversibility. In Sec. 5 we present numerical results for representative driving protocols. Finally, Sec. 6 summarizes our conclusions. Technical derivations and additional details are collected in the Appendices.

2 Autonomous clock model and reduced dynamics

2.1 Target protocol and STA benchmark

We consider a parametric harmonic oscillator (system) with canonical variables (x, p) and mass m . In the standard control description one prescribes a time-dependent frequency schedule $\omega(t)$ and studies the unitary generated by

$$H_{\text{bare}}(t) = \frac{p^2}{2m} + \frac{m}{2} \omega^2(t) x^2. \quad (1)$$

The time-dependent quantum harmonic oscillator provides a canonical setting to study the transition between adiabatic and sudden driving regimes [20]. For a given schedule $\omega(t)$, a shortcut-to-adiabaticity (STA) protocol consists in engineering a modified driving frequency $\Omega(t)$ such that, with t treated as an external classical parameter, the evolution reproduces the desired adiabatic mapping in finite time. In the present manuscript we use the familiar STA construction

$$H_{\text{STA}}(t) = \frac{p^2}{2m} + \frac{m}{2} \bar{\Omega}^2(t) x^2, \quad (2)$$

with

$$\bar{\Omega}^2(t) = \omega^2(t) + \frac{1}{2} \frac{\ddot{\omega}(t)}{\omega(t)} - \frac{3}{4} \left(\frac{\dot{\omega}(t)}{\omega(t)} \right)^2. \quad (3)$$

Similar STA constructions arise in other systems whose dynamics reduce to harmonic oscillators with time-dependent frequencies, such as electromagnetic modes in cavities with moving boundaries [21].

We assume that the driving is well-behaved at the endpoints (in particular, first and second derivatives vanish at $t = t_i$ and $t = t_f$) so that the initial and final instantaneous frequencies are unambiguously defined. In what follows, the STA evolution associated with $\bar{\Omega}(t)$ will serve as the *target* protocol.

2.2 Autonomous implementation with a quantum clock

To formulate time dependence from first principles, we replace the external parameter t by an explicit clock degree of freedom. The clock is modeled as a single pointer coordinate X with conjugate momentum P , evolving freely with mass M . The autonomous system–clock Hamiltonian is taken to be

$$H = \frac{p^2}{2m} + \frac{m}{2} \Omega^2[X] x^2 + \frac{P^2}{2M}. \quad (4)$$

Here $\Omega^2[X]$ is a smooth function of the clock coordinate, chosen so that along a prescribed mean clock trajectory $\bar{X}(t)$ the system experiences the target STA schedule,

$$\Omega^2[\bar{X}(t)] = \bar{\Omega}^2(t). \quad (5)$$

We will assume an initially uncorrelated state at $t = t_i$,

$$\rho_{\text{tot}}(t_i) = \rho_S(t_i) \otimes \rho_C(t_i), \quad (6)$$

and define the reduced state of the oscillator at t_f by tracing out the clock,

$$\rho_S(t_f) = \text{Tr}_C \left[U(t_f, t_i) \rho_{\text{tot}}(t_i) U^\dagger(t_f, t_i) \right]. \quad (7)$$

The global evolution is unitary; any effective nonunitarity for the oscillator arises solely because the clock is discarded.

2.3 Influence functional representation

The reduced dynamics may be expressed with a Feynman–Vernon influence functional [6, 7]. In coordinate representation one can write

$$\rho_S(x_f, x'_f, t_f) = \int dx_i dx'_i \int Dx Dx' e^{\frac{i}{\hbar}(S_S[x] - S_S[x'])} e^{\frac{i}{\hbar}S_{IF}[x, x']} \rho_S(x_i, x'_i, t_i), \quad (8)$$

where S_S is the system action evaluated along the two paths, and S_{IF} encodes the effect of the clock after it is traced out. The full derivation (including the explicit path-integral representation for the trace over clock histories and the resulting expression for S_{IF}) is given in Appendix A.

We now expand the clock coordinate around a prescribed mean trajectory,

$$X(t) = \bar{X}(t) + \xi(t), \quad (9)$$

and retain the leading (linear) response of the frequency to clock fluctuations,

$$\Omega^2[X(t)] \simeq \Omega^2[\bar{X}(t)] + \left. \frac{d\Omega^2}{dX} \right|_{\bar{X}(t)} \xi(t) \equiv \bar{\Omega}^2(t) + V(t) \xi(t), \quad (10)$$

where

$$V(t) = \left. \frac{d\Omega^2}{dX} \right|_{\bar{X}(t)}. \quad (11)$$

At this order the influence functional takes the standard Gaussian form [22]

$$S_{IF}[x, x'] = S_D[x, x'] + i S_N[x, x'], \quad (12)$$

with dissipation and noise contributions governed by the clock commutator and anticommutator kernels (definitions and explicit expressions are collected in Appendix A and Appendix B).

2.4 Noise-dominated single-parameter reduction

For a free pointer clock, the Heisenberg evolution of ξ is linear,

$$\xi(t) = \hat{\xi} + \frac{\hat{P}}{M} t, \quad (13)$$

and the clock kernels become simple functions of the clock state (Appendix B). In particular,

$$D(t, t') = i \langle [\xi(t), \xi(t')] \rangle \theta(t - t') = \frac{\hbar}{M} (t - t') \theta(t - t'), \quad (14)$$

$$N(t, t') = \langle \{ \xi(t), \xi(t') \} \rangle = 2 \langle \hat{\xi}^2 \rangle + \frac{2}{M^2} \langle \hat{P}^2 \rangle t t'. \quad (15)$$

In the regime of interest here we make two simplifications that lead to a compact reduced description: (i) we focus on clock states for which the term proportional to $\langle \hat{P}^2 \rangle$ dominates the noise kernel, so that the tt' structure of $N(t, t')$ is the leading contribution; and (ii) we work in a noise-dominated approximation in which the dissipative contribution S_D is neglected at leading order (see Appendix C for details and the resulting representation).

With these assumptions the noise functional factorizes as

$$S_N[x, x'] \simeq \frac{m^2}{8\hbar} \sigma_v^2 \left[\int_{t_i}^{t_f} dt t V(t) (x^2(t) - x'^2(t)) \right]^2, \quad \sigma_v^2 = \frac{\langle \hat{P}^2 \rangle}{M^2}. \quad (16)$$

Using a Hubbard–Stratonovich representation (Appendix C), one obtains

$$e^{\frac{i}{\hbar} S_{IF}[x, x']} \simeq \int dv P(v) \exp \left[-\frac{imv}{2\hbar} \int_{t_i}^{t_f} dt t V(t) (x^2(t) - x'^2(t)) \right], \quad (17)$$

where $P(v)$ is a Gaussian measure with $\langle v \rangle = 0$ and $\langle v^2 \rangle = \sigma_v^2$.

Equation (17) shows that the reduced dynamics can be written as an average over unitary evolutions labeled by a single real parameter v . Equivalently,

$$\rho_S(t_f) \simeq \int dv P(v) U_v(t_f, t_i) \rho_S(t_i) U_v^\dagger(t_f, t_i), \quad (18)$$

where U_v is the oscillator unitary generated by a parametric Hamiltonian with an effective, v -dependent frequency

$$\Omega^2(t) = \Omega^2[\bar{X}(t)] + V(t) v t \equiv \bar{\Omega}^2(t) + v \delta\Omega^2(t), \quad (19)$$

$$\delta\Omega^2(t) = t V(t). \quad (20)$$

For each fixed v the oscillator evolution is unitary; the reduced state becomes mixed only after averaging over v , i.e. after discarding the clock.

2.5 Assumptions and regime of validity

For clarity, we summarize the assumptions behind Eqs. (18)–(19):

- **Closed global dynamics.** The combined system (oscillator + clock) evolves unitarily; reduced nonunitarity arises only from tracing out the clock, Eq. (7).
- **Minimal clock model.** The clock is represented by a single free pointer degree of freedom with Hamiltonian $P^2/2M$.
- **Weak clock fluctuations.** We expand around a prescribed mean trajectory $X(t) = \bar{X}(t) + \xi(t)$ and retain only the leading (linear) response of $\Omega^2[X]$ to ξ , Eq. (10).
- **Noise-dominated approximation.** We neglect the dissipative influence contribution S_D at leading order, keeping only the noise functional S_N .
- **Single-parameter reduction.** We focus on the dominant tt' contribution in the noise kernel, yielding the factorized form Eq. (16) and the single Gaussian parameter v with variance $\sigma_v^2 = \langle \hat{P}^2 \rangle / M^2$.
- **Well-defined endpoints.** Protocols are assumed to have well-defined asymptotic frequencies at t_i, t_f , so that the target STA evolution is unambiguously defined.

3 Unitary dynamics for single trajectory

In the noise-dominated regime, the clock-traced output at t_f is a random-unitary mixture

$$\bar{\rho}_S(t_f) \simeq \int dv P(v) \rho_v(t_f), \quad \rho_v(t_f) = U_v(t_f, t_i) \rho_S(t_i) U_v^\dagger(t_f, t_i), \quad (21)$$

where for each realization v the oscillator evolves under the quadratic Hamiltonian

$$H_v(t) = \frac{p^2}{2m} + \frac{m}{2} \Omega_v^2(t) x^2, \quad \Omega_v^2(t) = \bar{\Omega}^2(t) + v \delta\Omega^2(t), \quad (22)$$

with $\delta\Omega^2(t) = tV(t)$ (Sec. 2.4). For each fixed v the evolution is unitary and Gaussian-preserving; nonunitarity arises only after averaging over v .

3.1 Symplectic evolution of the quadratures

Define the quadrature vector and symplectic form

$$\mathbf{R} \equiv (x, p)^\top, \quad J = \begin{pmatrix} 0 & 1 \\ -1 & 0 \end{pmatrix}, \quad [x, p] = i\hbar. \quad (23)$$

The Heisenberg equations generated by Eq. (22) are linear,

$$\frac{d}{dt} \mathbf{R}(t) = A_v(t) \mathbf{R}(t), \quad A_v(t) = \begin{pmatrix} 0 & 1/m \\ -m\Omega_v^2(t) & 0 \end{pmatrix}, \quad (24)$$

so there exists a fundamental matrix $S_v(t)$ such that

$$\mathbf{R}(t) = S_v(t) \mathbf{R}(t_i), \quad (25)$$

$$\frac{d}{dt} S_v(t) = A_v(t) S_v(t), \quad S_v(t_i) = \mathbb{I}_2. \quad (26)$$

For all t , $S_v(t)$ is symplectic,

$$S_v^\top(t) J S_v(t) = J, \quad (27)$$

hence $S_v(t) \in Sp(2, \mathbb{R})$ and $\det S_v(t) = 1$. We write $S_v \equiv S_v(t_f)$ for the final-time map.

Equivalently, $S_v(t)$ can be parametrized by two classical solutions u_v, w_v of

$$\ddot{y} + \Omega_v^2(t) y = 0 \quad (28)$$

with initial data $u_v(t_i) = 1, \dot{u}_v(t_i) = 0$ and $w_v(t_i) = 0, \dot{w}_v(t_i) = 1$, giving

$$S_v(t) = \begin{pmatrix} u_v(t) & \frac{1}{m} w_v(t) \\ m\dot{u}_v(t) & \dot{w}_v(t) \end{pmatrix}. \quad (29)$$

This representation makes transparent how each unitary trajectory acts linearly on (x, p) .

3.2 Symplectic map and Bogoliubov coefficients

For each realization v , the oscillator Hamiltonian $H_v(t)$ is quadratic, hence the Heisenberg evolution of the quadratures $\mathbf{R} = (x, p)^\top$ is linear:

$$\mathbf{R}(t_f) = S_v \mathbf{R}(t_i), \quad S_v \in Sp(2, \mathbb{R}), \quad S_v^\top J S_v = J, \quad (30)$$

with $J = \begin{pmatrix} 0 & 1 \\ -1 & 0 \end{pmatrix}$. At the endpoint t_f we introduce the ladder operator associated with the instantaneous frequency $\omega_f = \bar{\Omega}(t_f)$,

$$a_f = \sqrt{\frac{m\omega_f}{2\hbar}} x + i\sqrt{\frac{1}{2\hbar m\omega_f}} p, \quad (31)$$

so that $H_f = \hbar\omega_f(a_f^\dagger a_f + \frac{1}{2})$. Any symplectic map S_v therefore induces an equivalent Bogoliubov transformation on a_f ,

$$U_v^\dagger a_f U_v = \alpha_v a_f + \beta_v a_f^\dagger, \quad |\alpha_v|^2 - |\beta_v|^2 = 1, \quad (32)$$

and conversely (α_v, β_v) uniquely determine S_v .

Writing $S_v = \begin{pmatrix} a & b \\ c & d \end{pmatrix}$ in the (x, p) basis, a direct substitution of Eq. (31) into $\mathbf{R} \mapsto S_v \mathbf{R}$ gives the explicit dictionary

$$\alpha_v = \frac{1}{2} \left[a + d + i \left(\frac{c}{m\omega_f} - m\omega_f b \right) \right], \quad (33)$$

$$\beta_v = \frac{1}{2} \left[a - d + i \left(\frac{c}{m\omega_f} + m\omega_f b \right) \right], \quad (34)$$

which automatically satisfies $|\alpha_v|^2 - |\beta_v|^2 = 1$ whenever $S_v^\top J S_v = J$. This identification provides a transparent physical interpretation: β_v is the *squeezing/parametric excitation* generated by the v -dependent modulation. In particular, for a vacuum input one has $\langle n \rangle_v = \langle a_f^\dagger a_f \rangle_v = |\beta_v|^2$, and the excess final energy is $\Delta E(v) = \hbar\omega_f |\beta_v|^2$.

In the small-noise regime relevant for the clock-induced mixture, the dependence on v is perturbative,

$$\beta_v = iv \beta_1 + O(v^2), \quad (35)$$

so that $\overline{\langle n \rangle} = \int dv P(v) |\beta_v|^2 \simeq \sigma_v^2 |\beta_1|^2$. Hence $|\beta_1|$ quantifies the *susceptibility* of the target protocol to the clock-induced stochastic modulation, and it is the natural dimensionless control parameter behind the TUR plots shown below. The construction of S_v and its controlled expansion in v (including how to preserve symplecticity order by order) is provided in Appendix D, together with an explicit consistency check reproducing the vacuum/coherent Bogoliubov formulas from the symplectic overlap expressions in Appendix F.

4 Observables, clock averages, and TUR

In the noise-dominated regime the reduced output at t_f is the random-unitary mixture

$$\bar{\rho}_S(t_f) \simeq \int dv P(v) \rho_v(t_f), \quad \rho_v(t_f) = U_v \rho_S(t_i) U_v^\dagger, \quad (36)$$

with $P(v)$ Gaussian (Sec. 2.4). For each fixed v , U_v is generated by the quadratic Hamiltonian Eq. (19) and therefore maps Gaussian states to Gaussian states (Sec. 3).

In this section we define the figures of merit used to quantify the deviation from the target STA trajectory ($v = 0$), and we show how their clock averages can be evaluated analytically in a controlled small-noise regime.

4.1 Energy deviation and its clock-induced fluctuations

As an energetic diagnostic at the endpoint we use the instantaneous oscillator Hamiltonian

$$H_f = \frac{p^2}{2m} + \frac{m\omega_f^2}{2} x^2 = \frac{1}{2} \mathbf{R}^\top G_f \mathbf{R}, \quad G_f = \text{diag} \left(m\omega_f^2, \frac{1}{m} \right), \quad (37)$$

where $\omega_f \equiv \bar{\Omega}(t_f)$ and $\mathbf{R} = (x, p)^\top$.

For each realization v we define the *energetic deviation from the target* as

$$\Delta E(v) \equiv \langle H_f \rangle_v - \langle H_f \rangle_0, \quad (38)$$

and its clock average

$$\overline{\Delta E} \equiv \int dv P(v) \Delta E(v). \quad (39)$$

We quantify energetic ‘‘fluctuations’’ in two distinct senses. First, each unitary trajectory ρ_v generally has nonzero *quantum* energy uncertainty at the endpoint. We therefore define the excess (clock-induced) quantum variance

$$\sigma_E^2(v) \equiv \text{Var}_{\rho_v}(H_f) - \text{Var}_{\rho_0}(H_f), \quad \overline{\sigma_E^2} \equiv \int dv P(v) \sigma_E^2(v), \quad (40)$$

which vanishes in the ideal target evolution and isolates the additional uncertainty produced by the clock.

Second, the clock also induces a *classical* spread across trajectories in the mean energy,

$$\text{Var}(\langle H_f \rangle_v) \equiv \int dv P(v) \langle H_f \rangle_v^2 - \left(\int dv P(v) \langle H_f \rangle_v \right)^2, \quad (41)$$

which we use as an auxiliary diagnostic (Appendix E). For Gaussian inputs, both $\langle H_f \rangle_v$ and $\text{Var}_{\rho_v}(H_f)$ admit closed expressions in terms of the output first and second moments (Appendix E).

4.2 Irreversibility and target overlap

In our setting, the global evolution (system + clock) is unitary, and the only source of irreversibility for the controlled system is the coarse-graining associated with discarding the clock. In the noise-dominated regime, the reduced output at t_f is the random-unitary mixture

$$\bar{\rho} \equiv \int dv P(v) \rho_v, \quad \rho_v \equiv U_v \rho_i U_v^\dagger, \quad (42)$$

and we take $\rho_0 \equiv \rho_{v=0}$ as the target output.

A natural information-theoretic measure of mixing is the purity

$$\mathcal{P} \equiv \text{Tr}(\bar{\rho}^2), \quad \mathcal{P}_0 \equiv \text{Tr}(\rho_0^2), \quad (43)$$

and we define the associated Rényi-2 entropy $S_2(\rho) \equiv -\ln \text{Tr}(\rho^2)$ and its increment

$$\Delta S_2 \equiv S_2(\bar{\rho}) - S_2(\rho_0) = -\ln \left(\frac{\mathcal{P}}{\mathcal{P}_0} \right) \geq 0. \quad (44)$$

While the von Neumann entropy increase $S(\bar{\rho}) - S(\rho_0)$ is a natural notion of entropy production, S_2 is particularly convenient here because it is analytically tractable and directly tied to Gaussian overlap formulas. When the target output ρ_0 is pure, ΔS_2 also provides a conservative proxy for the true entropy increase since $S(\bar{\rho}) \geq S_2(\bar{\rho})$ and $S(\rho_0) = S_2(\rho_0) = 0$.

To quantify closeness to the target we use the normalized Hilbert–Schmidt overlap

$$F_{\text{HS}} \equiv \frac{\text{Tr}(\rho_0 \bar{\rho})}{\text{Tr}(\rho_0^2)} = \frac{1}{\mathcal{P}_0} \int dv P(v) \text{Tr}(\rho_0 \rho_v), \quad (45)$$

which coincides with the usual fidelity whenever ρ_0 is pure and is especially convenient because it reduces clock averages to Gaussian integrals over overlaps.

A key point is that purity loss and target overlap are not independent. By Cauchy–Schwarz for the Hilbert–Schmidt inner product,

$$[\text{Tr}(\rho_0 \bar{\rho})]^2 \leq \text{Tr}(\rho_0^2) \text{Tr}(\bar{\rho}^2) = \mathcal{P}_0 \mathcal{P}. \quad (46)$$

Dividing by \mathcal{P}_0^2 gives the universal bound

$$F_{\text{HS}}^2 \leq \frac{\mathcal{P}}{\mathcal{P}_0} \iff -2 \ln F_{\text{HS}} \geq \Delta S_2, \quad (47)$$

which expresses a model-independent tradeoff: achieving large overlap with the target output requires the clock-traced state to remain nearly pure.

4.3 Closed clock averages in the small-noise regime

When the relevant weight of $P(v)$ lies in the regime where a quadratic expansion of the log-overlap kernel is accurate, the v -integrals for \mathcal{P} and F_{HS} can be performed analytically. Writing $\sigma_v^2 \equiv \langle v^2 \rangle$ and denoting by a, b, c the protocol- and input-dependent coefficients defined in Appendix E, one finds

$$\mathcal{P} \simeq \frac{\mathcal{P}_0}{\sqrt{(1 + a\sigma_v^2)^2 - (c\sigma_v^2)^2}} \exp\left[\frac{b^2\sigma_v^2(1 + (a+c)\sigma_v^2)}{(1 + a\sigma_v^2)^2 - (c\sigma_v^2)^2}\right], \quad (48)$$

$$F_{\text{HS}} \simeq \frac{1}{\sqrt{1 + a\sigma_v^2}} \exp\left(\frac{b^2\sigma_v^2}{2[1 + a\sigma_v^2]}\right). \quad (49)$$

In many situations (in particular when the target $v = 0$ trajectory is a stationary point of the overlap kernel) one has $b = 0$, and (48)–(49) reduce to pure square-root forms.

Finally, the energetic deviation also scales as $\overline{\Delta E} = \chi_E \sigma_v^2 + O(\sigma_v^4)$, with an explicit susceptibility χ_E given in Appendix E. Eliminating σ_v^2 between $\overline{\Delta E}$ and ΔS_2 yields

$$\Delta S_2 = \frac{a}{\chi_E} \overline{\Delta E} + O(\sigma_v^4), \quad (50)$$

so that the universal inequality Eq. (47) becomes, in the controlled small-noise regime,

$$-\ln F_{\text{HS}} \geq \frac{1}{2} \Delta S_2 \simeq \frac{a}{2\chi_E} \overline{\Delta E}, \quad (51)$$

which is a geometric precision-irreversibility tradeoff: improving precision (larger overlap with the target) requires suppressing the irreversibility induced by discarding the clock, and this same irreversibility controls the energetic deviation from the target STA outcome.

TUR-type tradeoff. Beyond the universal precision–irreversibility inequality Eq. (47), we also introduce a thermodynamic-uncertainty-type figure of merit that combines (i) irreversibility due to discarding the clock and (ii) energetic precision at the endpoint. We use the linear-entropy production

$$S_L \equiv 1 - \frac{\mathcal{P}}{\mathcal{P}_0} \geq 0, \quad (52)$$

and define the TUR ratio (see Appendix G)

$$\mathcal{R}_E \equiv S_L \frac{\overline{\sigma_E^2}}{\overline{\Delta E}^2}. \quad (53)$$

In the noise-dominated small-noise regime (where the random-unitary reduction is controlled) we find that \mathcal{R}_E approaches a protocol-independent constant for the benchmark families studied below (vacuum and displaced vacuum), namely

$$\mathcal{R}_E \geq 2 + O(\sigma_v^2), \quad (54)$$

for the vacuum state and

$$\mathcal{R}_E \geq f(\mu) + O(\sigma_v^2), \quad (55)$$

for coherent states with annihilation operator eigenvalue μ , where $f(\mu)$ is an asymptotically decreasing function in $|\mu|$ (see Appendix G), with saturation at leading order as $\sigma_v^2 \rightarrow 0$. Equations (54) and (55) are the TUR statements we test numerically and plot in the following section.

5 Numerical tests and examples

We studied our model for two different frequency evolution protocols, one standard in toy-models for tabletop experiments [23, 24] and the other borrowed from cosmological applications [25, 26]. We call them "finite" and "infinite" time protocols respectively.

5.1 Finite time protocol

The frequency schedule for this case is

$$\omega^2(t) = \omega_i^2 + (\omega_f^2 - \omega_i^2) [10s^3 - 15s^4 + 6s^5], \quad (56)$$

with $s = \frac{t}{\tau}$. This protocol begins at $s = 0$ and ends at $s = 1$, satisfying $\dot{\omega}(0) = \dot{\omega}(1) = 0$ and $\ddot{\omega}(0) = \ddot{\omega}(1) = 0$ and also the Hamiltonian initial and final conditions. The protocol and its STA are plotted in Figure 1.

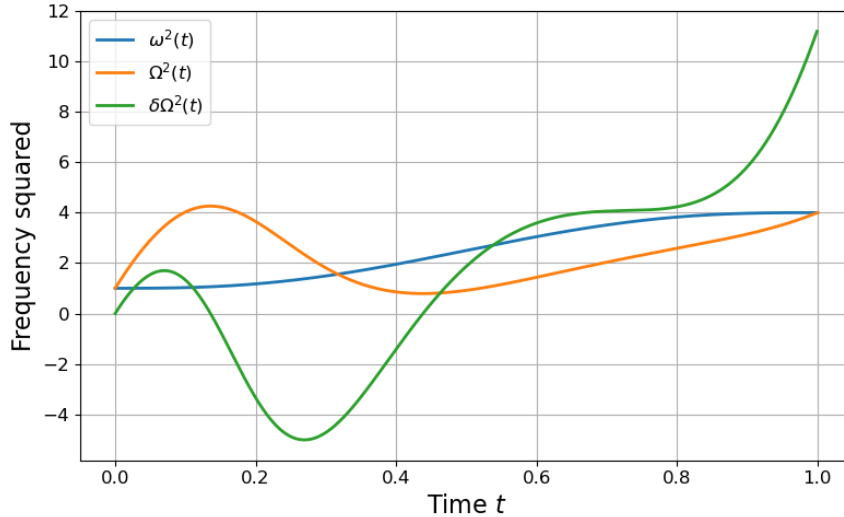


Figure 1: Frequency protocols for the finite-time driving schedule. The blue curve shows the prescribed frequency squared $\omega^2(t)$ defined in Eq. (56), which smoothly interpolates between the initial value ω_i and the final value ω_f during a total duration τ . The orange curve shows the corresponding shortcut-to-adiabaticity (STA) frequency $\Omega^2(t)$ constructed from Eq. (3), which guarantees that the oscillator follows the adiabatic mapping in finite time when time is treated as an external parameter. The green curve shows the STA deviation $\delta\Omega^2$ as defined in Eq. (20). Frequencies are shown in units where $\omega_i = 1$ and $\omega_f = 2$, and time is measured in units of the protocol duration τ .

The figures of merit and TUR ratio for the finite time protocol are plotted in Figure (2). For the α_1 and β_1 coefficients, we observe the typical $\sim \frac{1}{\tau}$ behavior for short τ . For long τ we observe the other typical behavior, $\sim e^{-c_1\tau}$ for β_1 (real and imaginary parts) and $\sim e^{c_2\tau}$ for α_1 , with c_1 and c_2 positive constants. For the coherent states, where $\mu \neq 0$, both purity and fidelity reach a maximum for a critical τ and then

decrease monotonically. The case where $\mu = 0$, the vacuum, tends asymptotically to a maximum value. The TUR ratio \mathcal{R}_E is a complicated function that depends not only on $|\mu|$ and τ , but also on the phase of μ and has some resonances where particle absorption or emission occurs. Nevertheless, it has a strictly positive minimum that is asymptotically decreasing on its $|\mu|$ dependence. Given that controlling the exact phase of the initial state can be challenging, we believe that the physical meaningful quantity is the average, so we computed the μ -phase averaged TUR ratio \mathcal{R}_E , where the decreasing $|\mu|$ dependence is clear (see Figure 2).

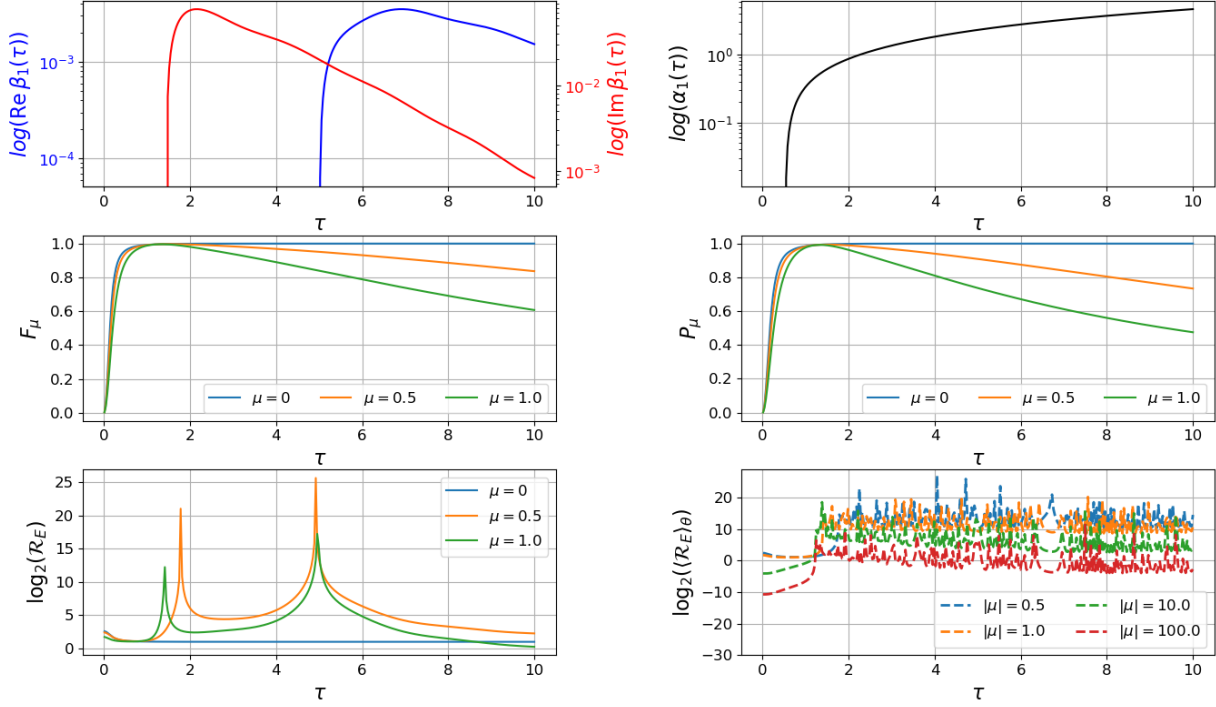


Figure 2: Figures of merit for the finite-time protocol as functions of the protocol duration τ . Top panels: logarithm of the real and imaginary parts of the Bogoliubov coefficient β_1 (left) and logarithm of α_1 (right), which characterize parametric excitations produced by the driving. Middle panels: fidelity with the target STA state (left) and purity of the reduced oscillator state (right), quantifying precision and irreversibility induced by discarding the clock degree of freedom. Bottom panels: logarithm of the thermodynamic-uncertainty-type ratio \mathcal{R}_E defined in Eq. (53) for different coherent-state amplitudes μ (left), and the phase-averaged ratio as a function of $|\mu|$ (right). These results illustrate the crossover between strong nonadiabatic effects at short durations and suppressed excitations in the slow-driving regime.

5.2 Infinite time protocol

The standard infinite-time protocol in cosmology is

$$\omega^2(t) = \frac{\omega_f^2 + \omega_i^2}{2} + \left(\frac{\omega_f^2 - \omega_i^2}{\pi} \right) \arctan(s) \quad (57)$$

with $s = \frac{t}{\tau}$. This protocol begins at $s = -\infty$ and ends at $s = \infty$, satisfying $\lim_{t \rightarrow -\infty} \dot{\omega}(t) = \lim_{t \rightarrow +\infty} \dot{\omega}(t) = 0$ and $\lim_{t \rightarrow -\infty} \ddot{\omega}(t) = \lim_{t \rightarrow +\infty} \ddot{\omega}(t) = 0$ and also the Hamiltonian initial and final conditions. The protocol and its STA are plotted in Figure 3.

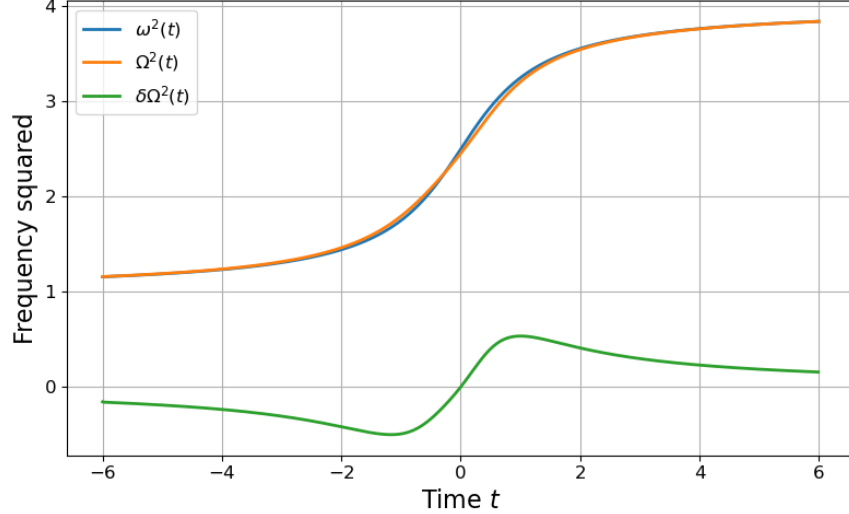


Figure 3: Frequency protocols for the infinite-time driving schedule defined in Eq. (57). The blue curve shows a time window of the bare frequency squared $\omega^2(t)$, which asymptotically approaches constant values at early and late times. The orange curve shows the shortcut-to-adiabaticity frequency $\bar{\Omega}^2(t)$ obtained from Eq. (3), while the green curve shows the corresponding STA deviation $\delta\Omega^2$ as defined in Eq. (20). As in Fig. 1, the STA protocol modifies the instantaneous frequency so that the system reproduces the adiabatic mapping in finite time. Frequencies are plotted in units where $\omega_i = 1$ and $\omega_f = 2$, with time measured in units of τ .

The figures of merit and TUR ratio for the infinite time protocol are plotted in Figure (4). For the α_1 and β_1 coefficients, we observe the typical $\sim \frac{1}{\tau}$ behavior for short τ . For long τ we met numerical stability issues due to the regularization needed in the phase of the oscillatory integrals. Nevertheless, analytical approximations indicate that we should observe an exponential decay for β_1 (real and imaginary parts) in the long- τ regime. For the coherent states studied, both purity and fidelity tend asymptotically towards a maximum. The TUR ratio \mathcal{R}_E is again a complicated function that depends not only on $|\mu|$ and τ , but also on the phase of μ (see Appendix G) and has some resonances where particle absorption or emission occurs. Nevertheless, it has a strictly positive minimum that is asymptotically decreasing on its $|\mu|$ dependence. Given that controlling the exact phase of the initial state can be challenging, we believe that the physical meaningful quantity is the average, so we computed the μ -phase averaged TUR ratio \mathcal{R}_E , where the decreasing $|\mu|$ dependence is clear (see Figure 4).

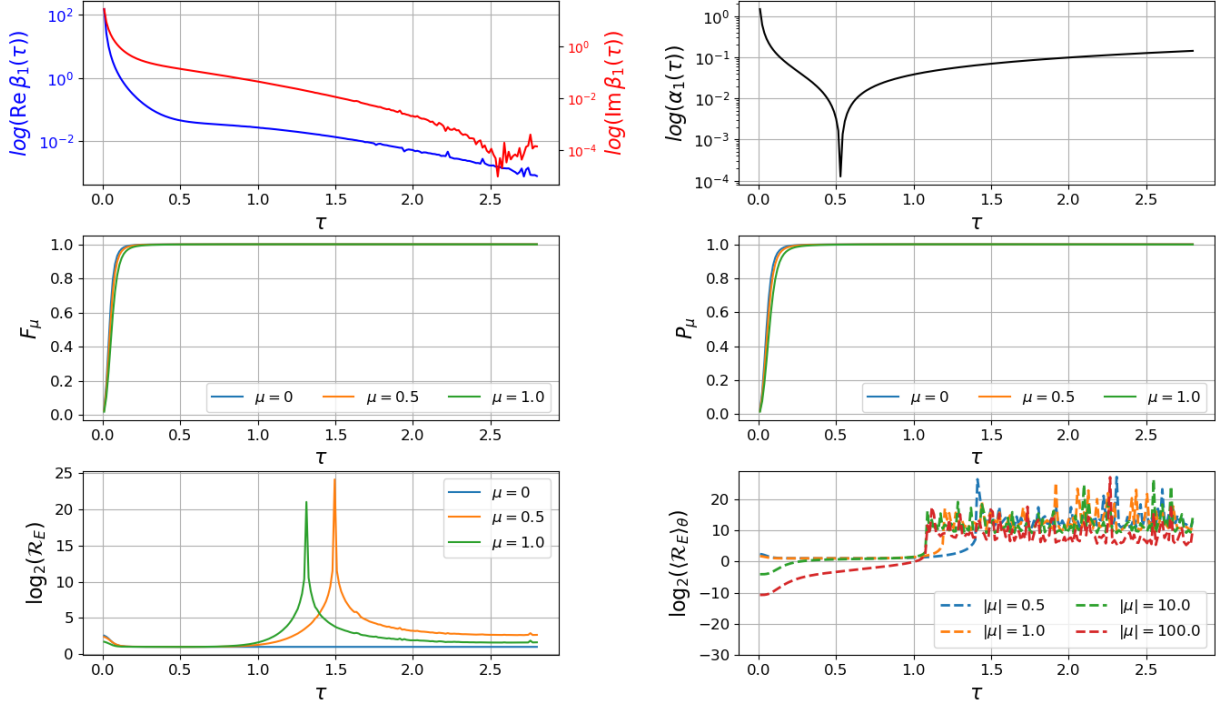


Figure 4: Same quantities as in Fig. 2 but for the infinite-time driving protocol defined in Eq. (57). The top panels show the dependence on the characteristic timescale τ of the (first order expansion) Bogoliubov coefficients α_1 and β_1 , the middle panels the fidelity with the target STA state and the purity of the reduced oscillator state, and the bottom panels the thermodynamic-uncertainty-type ratio \mathcal{R}_E for different values of the adiabatic parameter μ and its averaged counterpart in logarithmic scale. For short times the dynamics exhibits strong non-adiabatic excitations characterized by $|\beta_1| \sim \frac{1}{\tau}$, while increasing τ suppresses excitations and improve fidelity. The TUR ratio remains bounded from below, illustrating the trade-off between energetic fluctuations and irreversibility induced by tracing out the clock.

6 Conclusions and outlook

Time-dependent Hamiltonians are an indispensable effective language for quantum control and finite-time thermodynamic strokes. A fully closed microscopic description, however, must be autonomous: the apparent schedule $H(t)$ is generated by extra degrees of freedom that function as a time reference, and the controlled system becomes correlated with that reference. The central message of this work is that, even when the global dynamics is perfectly unitary and the target protocol is engineered to suppress deterministic nonadiabaticity (as in STA), discarding the clock generically produces an effectively open evolution for the system. This induces unavoidable decoherence and a spread of operational outcomes that are intrinsic to time-programmed dynamics.

Concretely, we studied a parametric harmonic oscillator driven by a STA target and implemented autonomously by coupling the oscillator frequency to a minimal pointer clock, building on Ref. [5]. Starting from the unitary system–clock dynamics and tracing out the clock with a Feynman–Vernon influence functional, we identified a noise-dominated regime in which the reduced dynamics at the final time is a *random-unitary* mixture, $\bar{\rho} = \int dv P(v) \rho_v$, labelled by a single Gaussian clock parameter v . This provides a transparent microscopic origin for an “error model” of time-dependent control that does not require adding stochasticity by hand.

Within this reduced description we quantified three operational consequences of clock-induced system–clock correlations: (i) an energetic deviation from the target STA outcome and its associated fluctuations, (ii) loss of overlap with the target trajectory (fidelity/precision), and (iii) loss of purity (irreversibility) of the

clock-traced state. For Gaussian inputs, the symplectic formulation makes these quantities computable in closed form (in a controlled small-noise regime), and it also clarifies the role of the Bogoliubov coefficient β : for each trajectory, $|\beta_v|^2$ is the parametric excitation (squeezing) generated by the v -dependent modulation, while $|\beta_1|$ (from $\beta_v = iv\beta_1 + O(v^2)$) is the *protocol susceptibility* to clock-induced timing uncertainty. This gives direct physical meaning to the quantity that appears in the numerical plots.

Our results complement and sharpen several related lines of work. A large literature on STA quantifies energetic and thermodynamic costs of fast driving and the tradeoff between speed and resources [27]. Separately, the quantum nature of control degrees of freedom has long been known to limit idealized control, since quantized controllers (e.g. laser modes) generically entangle with the system and induce errors when discarded [10, 11, 12, 15]. More recent approaches capture imperfect timekeeping by randomizing the duration of an otherwise time-independent operation [16, 17], and autonomous clock-driven dynamics has been developed in thermodynamic settings [18, 19]. The present work sits at the intersection of these themes, but differs in emphasis: we focus on *genuinely time-programmed Hamiltonian protocols* (here, an STA schedule) and derive the reduced stochastic description from a first-principles system–clock model. This allows us to express precision loss, purity loss, and energetic deviations in a unified way and to formulate a thermodynamic-uncertainty-type tradeoff between energetic fluctuations and irreversibility generated by discarding the clock.

Several extensions are natural. First, we worked in a noise-dominated approximation and neglected the dissipative kernel of the influence functional at leading order. Restoring it would incorporate systematic backaction/friction-like terms and enable a more complete non-Markovian reduced dynamics; in that setting, it is natural to revisit stochastic representations and their connection to unraveling-type descriptions. Second, while we provided analytic control for Gaussian inputs and small noise, the mixture $\bar{\rho}$ is generically non-Gaussian; extending the analysis to non-Gaussian resources (e.g. Schrödinger-cat superpositions) is a natural next step, both conceptually and for quantum-information applications. Third, our minimal clock can be generalized to more realistic clocks [28] (finite bandwidth, multi-mode, or explicitly thermodynamic clocks), and to regimes where the system significantly perturbs the clock, connecting with the growing literature on constrained clock-driven dynamics [19].

Beyond the present model, the general principle—that autonomous time dependence necessarily produces system–clock correlations and therefore limits idealized time-programmed unitaries—is directly relevant to high-precision coherent control and quantum information processing. Recent work has highlighted thermodynamic constraints on information gain and error correction [29]; our results provide a complementary, clock-induced mechanism by which irreversibility and fluctuations arise even without external environments, suggesting a route to principled performance bounds for time-scheduled quantum operations.

7 Acknowledgements

F.C. acknowledges funding by the European Union (EQC, 101149233).

Work supported in part by Universidad de Buenos Aires through Grant No. UBACYT 20020170100129BA, CONICET Grant No. PIP2017/19:11220170100817CO, and ANPCyT Grant No. PICT 2018: 03684.

A Influence functional for the system–clock model

In this Appendix we derive the influence functional representation used in Sec. 2.

A.1 Path-integral representation of the reduced state

The total Hamiltonian is

$$H = \frac{p^2}{2m} + \frac{m}{2}\Omega^2[X]x^2 + \frac{P^2}{2M}. \quad (4)$$

Assuming an initially factorized state $\rho_{\text{tot}}(t_i) = \rho_S(t_i) \otimes \rho_C(t_i)$, the reduced density matrix of the oscillator at t_f admits the (exact) double path-integral representation

$$\rho_S(x_f, x'_f, t_f) = \int dx_i dx'_i dX_i dX'_i dX_f \int_{\substack{x(t_f) = x_f \\ x'(t_f) = x'_f \\ X(t_f) = X_f \\ X'(t_f) = X'_f \\ x(t_i) = x_i \\ x'(t_i) = x'_i \\ X(t_i) = X_i \\ X'(t_i) = X'_i}} Dx Dx' DX DX' \times \exp\left\{\frac{i}{\hbar} \left(S_{SC}[x, X] - S_{SC}[x', X'] \right)\right\} \rho_C(X_i, X'_i, t_i) \rho_S(x_i, x'_i, t_i), \quad (58)$$

where the system–clock action is

$$S_{SC}[x, X] = \int_{t_i}^{t_f} dt \left[\frac{M}{2} \dot{X}^2 + \frac{m}{2} \dot{x}^2 - \frac{m}{2} \Omega^2[X] x^2 \right]. \quad (59)$$

A.2 Expansion around a mean clock trajectory

We expand the clock history around a prescribed mean trajectory,

$$X(t) = \bar{X}(t) + \xi(t), \quad (9)$$

and retain the leading correction in ξ . Writing

$$\Omega^2[X] \simeq \Omega^2[\bar{X}] + \left. \frac{d\Omega^2}{dX} \right|_{\bar{X}} \xi \equiv \bar{\Omega}^2(t) + V(t) \xi(t), \quad (10)$$

with $V(t)$ given by Eq. (11), the interaction term becomes

$$S_I[x, \xi] = -\frac{m}{2} \int_{t_i}^{t_f} dt V(t) \xi(t) x^2(t). \quad (60)$$

Tracing out the clock degrees of freedom yields the Feynman–Vernon influence functional,

$$e^{\frac{i}{\hbar} S_{IF}[x, x']} = \int D\xi D\xi' e^{\frac{i}{\hbar} (S_C[\xi] - S_C[\xi'])} e^{\frac{i}{\hbar} (S_I[x, \xi] - S_I[x', \xi'])} \rho_C(\xi_i, \xi'_i, t_i), \quad (61)$$

where $S_C[\xi] = \int dt \frac{M}{2} \dot{\xi}^2$ for the free pointer clock.

Because the clock is Gaussian (free) and the coupling is linear in ξ , S_{IF} is quadratic in the system coordinates and can be written as

$$S_{IF}[x, x'] = S_D[x, x'] + iS_N[x, x']. \quad (12)$$

A convenient explicit form is

$$S_D[x, x'] = \frac{m^2}{8} \int_{t_i}^{t_f} dt V(t) (x^2 - x'^2)(t) \int_{t_i}^{t_f} dt' V(t') D(t, t') (x^2 + x'^2)(t'), \quad (62)$$

$$S_N[x, x'] = \frac{m^2}{16} \int_{t_i}^{t_f} dt V(t) (x^2 - x'^2)(t) \int_{t_i}^{t_f} dt' V(t') N(t, t') (x^2 - x'^2)(t'), \quad (63)$$

with the kernels

$$D(t, t') = i \langle [\xi(t), \xi(t')] \rangle \theta(t - t'), \quad (64)$$

$$N(t, t') = \langle \{ \xi(t), \xi(t') \} \rangle. \quad (65)$$

The averages are taken in the initial clock state $\rho_C(t_i)$.

B Clock correlators and kernels

In this Appendix we compute the kernels $D(t, t')$ and $N(t, t')$ for the free pointer clock used in the main text.

B.1 Free pointer evolution

For the free clock Hamiltonian $H_C = P^2/2M$, the Heisenberg evolution of the pointer fluctuation is

$$\xi(t) = \hat{\xi} + \frac{\hat{P}}{M} t. \quad (13)$$

Using $[\hat{\xi}, \hat{P}] = i\hbar$, we find

$$[\xi(t), \xi(t')] = \left[\hat{\xi} + \frac{\hat{P}}{M} t, \hat{\xi} + \frac{\hat{P}}{M} t' \right] = \frac{i\hbar}{M} (t - t'), \quad (66)$$

$$\{\xi(t), \xi(t')\} = 2\hat{\xi}^2 + \frac{t+t'}{M} (\hat{\xi}\hat{P} + \hat{P}\hat{\xi}) + \frac{2}{M^2} \hat{P}^2 t t'. \quad (67)$$

For clock states that are parity-symmetric in ξ (or more generally for which $\langle \hat{\xi}\hat{P} + \hat{P}\hat{\xi} \rangle = 0$), this reduces to

$$\langle [\xi(t), \xi(t')] \rangle = \frac{i\hbar}{M} (t - t'), \quad (68)$$

$$\langle \{\xi(t), \xi(t')\} \rangle = 2\langle \hat{\xi}^2 \rangle + \frac{2}{M^2} \langle \hat{P}^2 \rangle t t'. \quad (69)$$

Substituting into Eqs. (64)–(65) yields the kernels quoted in the main text,

$$D(t, t') = \frac{\hbar}{M} (t - t') \theta(t - t'), \quad (70)$$

$$N(t, t') = 2\langle \hat{\xi}^2 \rangle + \frac{2}{M^2} \langle \hat{P}^2 \rangle t t'. \quad (71)$$

C Noise-dominated limit and Hubbard–Stratonovich reduction

Here we provide the steps leading from the influence functional to the single-parameter random-unitary form used in Sec. 2.4.

C.1 Factorization of the noise functional

Using the tt' contribution in $N(t, t')$,

$$N(t, t') \simeq \frac{2}{M^2} \langle \hat{P}^2 \rangle t t' \equiv 2\sigma_v^2 t t', \quad \sigma_v^2 = \frac{\langle \hat{P}^2 \rangle}{M^2}, \quad (72)$$

the noise functional (63) becomes

$$\begin{aligned} S_N[x, x'] &\simeq \frac{m^2}{16} \int dt V(t) \Delta(t) \int dt' V(t') (2\sigma_v^2 t t') \Delta(t') \\ &= \frac{m^2}{8} \sigma_v^2 \left[\int dt t V(t) \Delta(t) \right]^2, \quad \Delta(t) \equiv x^2(t) - x'^2(t), \end{aligned} \quad (73)$$

which is Eq. (16) (up to the overall $1/\hbar$ factor in $e^{\frac{i}{\hbar} S_{IF}}$).

C.2 Hubbard–Stratonovich representation

We use the Gaussian identity

$$e^{-\frac{1}{2}\sigma_v^2 I^2} = \int dv P(v) e^{ivI}, \quad P(v) = \frac{1}{\sqrt{2\pi\sigma_v^2}} e^{-\frac{v^2}{2\sigma_v^2}}, \quad (74)$$

which matches Eq. (17) in the main text with an explicit normalization. With

$$I[x, x'] = \frac{m}{2\hbar} \int_{t_i}^{t_f} dt t V(t) (x^2(t) - x'^2(t)), \quad (75)$$

the noise contribution satisfies

$$e^{-\frac{1}{2}\sigma_v^2 I^2} = \int dv P(v) e^{ivI}. \quad (76)$$

Neglecting the dissipative part S_D at leading order (noise-dominated approximation), we obtain

$$e^{\frac{i}{\hbar} S_{IF}[x, x']} \simeq \int dv P(v) \exp\left[-\frac{imv}{2\hbar} \int_{t_i}^{t_f} dt t V(t) (x^2(t) - x'^2(t))\right], \quad (77)$$

which is Eq. (17).

C.3 Random-unitary representation

For each fixed v , the exponent in Eq. (77) amounts to modifying the system action by a v -dependent quadratic term. This is equivalent to a unitary oscillator evolution with effective frequency

$$\Omega^2(t) = \bar{\Omega}^2(t) + v \delta\Omega^2(t), \quad \delta\Omega^2(t) = t V(t), \quad (78)$$

leading to the random-unitary channel representation

$$\rho_S(t_f) \simeq \int dv P(v) U_v(t_f, t_i) \rho_S(t_i) U_v^\dagger(t_f, t_i). \quad (79)$$

This decomposition makes clear that the reduced dynamics is a mixture of unitary trajectories (labeled by v); mixedness arises only after averaging over v , i.e. after discarding the clock degrees of freedom.

D Perturbative construction of the symplectic map S_v

In this Appendix we show how to expand $S_v(t_f)$ in v in a way that respects the symplectic constraint $S_v^\top J S_v = J$ order by order.

D.1 Interaction-picture (Dyson) expansion

Write

$$A_v(t) = A_0(t) + v A_1(t), \quad A_1(t) = \begin{pmatrix} 0 & 0 \\ -m \delta\Omega^2(t) & 0 \end{pmatrix}. \quad (80)$$

Let $S_0(t)$ be the fundamental matrix for $v = 0$:

$$\dot{S}_0(t) = A_0(t) S_0(t), \quad S_0(t_i) = \mathbb{I}_2. \quad (81)$$

Define the interaction-picture map

$$Y_v(t) \equiv S_0^{-1}(t) S_v(t), \quad Y_v(t_i) = \mathbb{I}_2. \quad (82)$$

Then Y_v satisfies

$$\dot{Y}_v(t) = v B(t) Y_v(t), \quad B(t) \equiv S_0^{-1}(t) A_1(t) S_0(t). \quad (83)$$

Because $B^\top J + JB = 0$, one has $B(t) \in \mathfrak{sp}(2, \mathbb{R})$ and hence $Y_v(t) \in Sp(2, \mathbb{R})$ for all v, t . The Dyson expansion gives

$$Y_v(t_f) = \mathbb{I}_2 + v \int_{t_i}^{t_f} dt_1 B(t_1) + v^2 \int_{t_i}^{t_f} dt_1 \int_{t_i}^{t_1} dt_2 B(t_1) B(t_2) + O(v^3). \quad (84)$$

Finally,

$$S_v(t_f) = S_0(t_f) Y_v(t_f), \quad (85)$$

which provides explicit integral expressions for the v -derivatives of S_v at $v = 0$.

D.2 Equivalent expansion via fundamental solutions

Alternatively, expand the fundamental solutions of $\ddot{y} + \Omega_v^2(t)y = 0$ as $u_v = u_0 + v u_1 + v^2 u_2 + \dots$ and $w_v = w_0 + v w_1 + v^2 w_2 + \dots$. Matching powers of v yields the driven hierarchy

$$\ddot{u}_0 + \bar{\Omega}^2 u_0 = 0, \quad u_0(t_i) = 1, \quad \dot{u}_0(t_i) = 0, \quad (86)$$

$$\ddot{u}_1 + \bar{\Omega}^2 u_1 = -\delta \Omega^2 u_0, \quad u_1(t_i) = \dot{u}_1(t_i) = 0, \quad (87)$$

$$\ddot{u}_2 + \bar{\Omega}^2 u_2 = -\delta \Omega^2 u_1, \quad u_2(t_i) = \dot{u}_2(t_i) = 0, \quad (88)$$

(and similarly for w_k with $w_0(t_i) = 0, \dot{w}_0(t_i) = 1$ and $w_{1,2}(t_i) = \dot{w}_{1,2}(t_i) = 0$). Substituting into

$$S_v(t) = \begin{pmatrix} u_v(t) & \frac{1}{m} w_v(t) \\ m \dot{u}_v(t) & \dot{w}_v(t) \end{pmatrix} \quad (89)$$

yields the perturbative symplectic map. The Wronskian identity $u_v \dot{w}_v - \dot{u}_v w_v = 1$ ensures symplecticity (up to the truncation order).

E Gaussian clock averages: energy, purity, and HS fidelity

This Appendix collects the technical steps leading to the closed expressions (48)–(51).

E.1 Moment propagation for fixed v

For each fixed v , the unitary U_v induces a symplectic map S_v on $\mathbf{R} = (x, p)^\top$,

$$\mathbf{R}(t_f) = S_v \mathbf{R}(t_i), \quad S_v \in Sp(2, \mathbb{R}), \quad (90)$$

hence a Gaussian input remains Gaussian. Writing the input mean vector and covariance at t_i as

$$\mathbf{d}_i \equiv \langle \mathbf{R}(t_i) \rangle, \quad V_i \equiv \frac{1}{2} \langle \{ \Delta \mathbf{R}(t_i), \Delta \mathbf{R}(t_i)^\top \} \rangle, \quad \Delta \mathbf{R} \equiv \mathbf{R} - \mathbf{d}, \quad (91)$$

the output moments for realization v are

$$\mathbf{d}_v = S_v \mathbf{d}_i, \quad V_v = S_v V_i S_v^\top. \quad (92)$$

We work perturbatively at fixed t_f and write

$$S_v = S_0 + v S^{(1)} + \frac{v^2}{2} S^{(2)} + O(v^3), \quad (93)$$

where $S^{(k)} \equiv \partial_v^k S_v|_{v=0}$. A symplecticity-preserving construction of these derivatives is given in Appendix D. This induces

$$\mathbf{d}_v = \mathbf{d}_0 + v\mathbf{d}^{(1)} + \frac{v^2}{2}\mathbf{d}^{(2)} + O(v^3), \quad \mathbf{d}^{(1)} = S^{(1)}\mathbf{d}_i, \quad \mathbf{d}^{(2)} = S^{(2)}\mathbf{d}_i, \quad (94)$$

$$V_v = V_0 + vV^{(1)} + \frac{v^2}{2}V^{(2)} + O(v^3), \quad (95)$$

with

$$V^{(1)} = S^{(1)}V_iS_0^\top + S_0V_i(S^{(1)})^\top, \quad (96)$$

$$V^{(2)} = S^{(2)}V_iS_0^\top + S_0V_i(S^{(2)})^\top + 2S^{(1)}V_i(S^{(1)})^\top. \quad (97)$$

E.2 Energy: mean deviation and clock-induced variance

With $H_f = \frac{1}{2}\mathbf{R}^\top G_f \mathbf{R}$ and $G_f = \text{diag}(m\omega_f^2, 1/m)$, a Gaussian state with moments (\mathbf{d}, V) satisfies

$$\langle H_f \rangle = \frac{1}{2} \text{Tr}(G_f V) + \frac{1}{2} \mathbf{d}^\top G_f \mathbf{d}. \quad (98)$$

Expanding $\langle H_f \rangle_v$ using (94)–(95) gives

$$\langle H_f \rangle_v = \langle H_f \rangle_0 + v E^{(1)} + \frac{v^2}{2} E^{(2)} + O(v^3), \quad (99)$$

$$E^{(1)} = \frac{1}{2} \text{Tr}(G_f V^{(1)}) + \mathbf{d}_0^\top G_f \mathbf{d}^{(1)}, \quad (100)$$

$$E^{(2)} = \frac{1}{2} \text{Tr}(G_f V^{(2)}) + (\mathbf{d}^{(1)})^\top G_f \mathbf{d}^{(1)} + \mathbf{d}_0^\top G_f \mathbf{d}^{(2)}. \quad (101)$$

Since $P(v)$ is even, $\int dv P(v) v = 0$ and $\int dv P(v) v^2 = \sigma_v^2$, hence

$$\overline{\Delta E} = \int dv P(v) (\langle H_f \rangle_v - \langle H_f \rangle_0) = \frac{\sigma_v^2}{2} E^{(2)} + O(\sigma_v^4). \quad (102)$$

The clock-induced variance across trajectories (defined in (40), which resembles a constancy [30]) reads

$$\text{Var}_v(H_f) = \sigma_v^2 (E^{(1)})^2 + O(\sigma_v^4), \quad (103)$$

because the mean shift is $O(\sigma_v^2)$ while the leading fluctuations come from the linear term.

E.3 Gaussian overlap kernel

For one-mode Gaussian states ρ_1, ρ_2 with moments (\mathbf{d}_1, V_1) and (\mathbf{d}_2, V_2) in the convention $[x, p] = i\hbar$, their Hilbert–Schmidt overlap is

$$\text{Tr}(\rho_1 \rho_2) = \frac{\hbar}{\sqrt{\det(V_1 + V_2)}} \exp\left[-\frac{1}{2}(\mathbf{d}_1 - \mathbf{d}_2)^\top (V_1 + V_2)^{-1} (\mathbf{d}_1 - \mathbf{d}_2)\right]. \quad (104)$$

Define the kernel $K(v, v') \equiv \text{Tr}(\rho_v \rho_{v'})$. Then

$$\mathcal{P} = \text{Tr}(\bar{\rho}_S^2) = \iint dv dv' P(v) P(v') K(v, v'), \quad F_{\text{HS}} = \frac{1}{\mathcal{P}_0} \int dv P(v) K(v, 0), \quad (105)$$

with $\mathcal{P}_0 \equiv K(0, 0) = \text{Tr}(\rho_0^2) = \hbar/\sqrt{\det(2V_0)}$.

E.4 Quadratic expansion of $-\log K(v, v')$ and evaluation of the v -integrals

Introduce $\Sigma(v, v') \equiv V_v + V_{v'}$ and $\Delta \mathbf{d}(v, v') \equiv \mathbf{d}_v - \mathbf{d}_{v'}$. From (104),

$$\log K(v, v') = \log \hbar - \frac{1}{2} \log \det \Sigma(v, v') - \frac{1}{2} \Delta \mathbf{d}^\top \Sigma^{-1} \Delta \mathbf{d}. \quad (106)$$

Using (94)–(95), to second order one needs

$$\Sigma(v, v') = 2V_0 + (v + v')V^{(1)} + \frac{v^2 + v'^2}{2} V^{(2)} + O(3), \quad (107)$$

$$\Delta \mathbf{d}(v, v') = (v - v') \mathbf{d}^{(1)} + O(2), \quad (108)$$

and in the displacement term it is sufficient to set $\Sigma^{-1} \rightarrow (2V_0)^{-1}$ at this order.

Writing the quadratic expansion in the symmetric form

$$-\log K(v, v') = -\log \mathcal{P}_0 + b(v + v') + \frac{1}{2} a(v^2 + v'^2) - c v v' + O(3), \quad (109)$$

one obtains the trace expressions

$$Q \equiv V_0^{-1} V^{(1)}, \quad (110)$$

$$b = \frac{1}{4} \text{Tr}(Q), \quad (111)$$

$$a = \frac{1}{4} \text{Tr}(V_0^{-1} V^{(2)}) - \frac{1}{8} \text{Tr}(Q^2) + \frac{1}{2} (\mathbf{d}^{(1)})^\top V_0^{-1} \mathbf{d}^{(1)}, \quad (112)$$

$$c = \frac{1}{8} \text{Tr}(Q^2) + \frac{1}{2} (\mathbf{d}^{(1)})^\top V_0^{-1} \mathbf{d}^{(1)}. \quad (113)$$

Exponentiating (109) yields the Gaussian approximation to the kernel,

$$K(v, v') \simeq \mathcal{P}_0 \exp \left[-b(v + v') - \frac{1}{2} a(v^2 + v'^2) + c v v' \right]. \quad (114)$$

Substituting into (105) reduces \mathcal{P} to a two-dimensional Gaussian integral and F_{HS} to a one-dimensional Gaussian integral, giving the closed forms (48)–(49). When $b = 0$ (stationary kernel), the exponentials drop out and the results reduce to pure square-root expressions.

E.5 Link between ΔS_2 and $\overline{\Delta E}$

In the small-noise regime, $\Delta S_2 = -\ln(\mathcal{P}/\mathcal{P}_0) = a\sigma_v^2 + O(\sigma_v^4)$ for $b = 0$, while (102) gives $\overline{\Delta E} = \chi_E \sigma_v^2 + O(\sigma_v^4)$ with

$$\chi_E \equiv \frac{1}{2} E^{(2)} = \frac{1}{4} \text{Tr}(G_f V^{(2)}) + \frac{1}{2} (\mathbf{d}^{(1)})^\top G_f \mathbf{d}^{(1)} + \frac{1}{2} \mathbf{d}_0^\top G_f \mathbf{d}^{(2)}. \quad (115)$$

This yields (50) in the main text.

F Bogoliubov–symplectic dictionary and consistency check

Here we show explicitly that the Bogoliubov description used in the vacuum/coherent calculations and the symplectic description used for generic Gaussian inputs are two representations of the same Gaussian unitary for each fixed v .

F.1 From Bogoliubov to a symplectic matrix in the target basis

At the final time, define the target ladder operator and corresponding quadratures by

$$a_T = e^{iI_f} a_f, \quad x = \sqrt{\frac{\hbar}{2m\omega_f}} (a_T + a_T^\dagger), \quad p = -i\sqrt{\frac{\hbar m\omega_f}{2}} (a_T - a_T^\dagger), \quad (116)$$

so that $H_f = \hbar\omega_f(a_T^\dagger a_T + \frac{1}{2})$. For a given noise realization v , the evolved annihilation operator is related to a_T by the Bogoliubov map

$$a(v) = \alpha_v^* a_T - \beta_v^* a_T^\dagger, \quad a^\dagger(v) = \alpha_v a_T^\dagger - \beta_v a_T, \quad |\alpha_v|^2 - |\beta_v|^2 = 1. \quad (117)$$

Introduce the shorthand $u \equiv \alpha_v^*$ and $w \equiv -\beta_v^*$, so that $a(v) = u a_T + w a_T^\dagger$. Then $a_T = u^* a(v) - w a^\dagger(v)$ and $a_T^\dagger = -w^* a(v) + u a^\dagger(v)$. Substituting these into Eq. (116) yields

$$x = \sqrt{\frac{\hbar}{2m\omega_f}} \left[(u^* - w^*) a(v) + (u - w) a^\dagger(v) \right], \quad (118)$$

$$p = -i\sqrt{\frac{\hbar m\omega_f}{2}} \left[(u^* + w^*) a(v) - (u + w) a^\dagger(v) \right]. \quad (119)$$

Now express $a(v)$, $a^\dagger(v)$ back in terms of the *same* quadratures (x, p) in the v -basis,

$$a(v) = \sqrt{\frac{m\omega_f}{2\hbar}} x + \frac{i}{\sqrt{2\hbar m\omega_f}} p, \quad a^\dagger(v) = \sqrt{\frac{m\omega_f}{2\hbar}} x - \frac{i}{\sqrt{2\hbar m\omega_f}} p, \quad (120)$$

and collect coefficients. One obtains a real linear map $\mathbf{R} = (x, p)^\top \mapsto S_v^{(T)} \mathbf{R}$ with

$$S_v^{(T)} = \begin{pmatrix} \operatorname{Re}(u + w) & \frac{1}{m\omega_f} \operatorname{Im}(u - w) \\ -m\omega_f \operatorname{Im}(u + w) & \operatorname{Re}(u - w) \end{pmatrix}, \quad u = \alpha_v^*, \quad w = -\beta_v^*. \quad (121)$$

Using $|\alpha_v|^2 - |\beta_v|^2 = 1$, it is straightforward to verify that $S_v^{(T)\top} J S_v^{(T)} = J$ (hence $S_v^{(T)} \in Sp(2, \mathbb{R})$). This establishes the equivalence: specifying (α_v, β_v) fixes the symplectic map $S_v^{(T)}$, and conversely.

F.2 Vacuum state in symplectic formalism

For the target vacuum $\rho_0 = |0\rangle_T \langle 0|$, the target covariance in the (x, p) basis is

$$V_0 = \frac{\hbar}{2} \begin{pmatrix} \frac{1}{m\omega_f} & 0 \\ 0 & m\omega_f \end{pmatrix}, \quad (122)$$

and for each v the output is a squeezed vacuum with covariance $V_v = S_v^{(T)} V_0 S_v^{(T)\top}$. The mean remains zero. Therefore the energy deviation is

$$\langle H_f \rangle_v - \langle H_f \rangle_0 = \frac{1}{2} \operatorname{Tr}(G_f(V_v - V_0)) = \hbar\omega_f |\beta_v|^2, \quad (123)$$

in agreement with the Bogoliubov result in the main text (obtained by normal ordering H_f in the $a(v)$ basis).

Moreover, the Hilbert–Schmidt overlap between two one-mode Gaussian states depends only on their first and second moments. For the vacuum case, $\mathbf{d}_v = 0$ and

$$\operatorname{Tr}(\rho_v \rho_{v'}) = \frac{\hbar}{\sqrt{\det(V_v + V_{v'})}}, \quad (124)$$

which, using the perturbative expansion $\beta_v \simeq iv\beta_1$ in the noise-dominated regime, yields

$$|\langle 0, v|0, 0 \rangle_T|^2 \simeq \exp\left[-\frac{1}{2}|\beta_1|^2 v^2\right], \quad |\langle 0, v|0, v' \rangle|^2 \simeq \exp\left[-\frac{1}{2}|\beta_1|^2 (v - v')^2\right], \quad (125)$$

which are exactly the Gaussian kernels used in the explicit Bogoliubov overlap calculation. Performing the v (and v, v') Gaussian averages then reproduces

$$F_0 = \frac{1}{\sqrt{1 + |\beta_1|^2 \sigma_v^2}}, \quad \mathcal{P}_0 = \frac{1}{\sqrt{1 + 2|\beta_1|^2 \sigma_v^2}}, \quad (126)$$

as quoted in Sec. The coherent-state case follows similarly: the covariance evolves as in the vacuum, while the mean is transported linearly by $S_v^{(T)}$, so all observables split into a covariance contribution (squeezing) plus a mean contribution (displacement).

G TUR

Because of computational difficulties, we formulate our TUR-type relation in terms of the linear-entropy production and compute it for initially coherent states in terms of the Bogoliubov coefficients:

$$\begin{aligned} S_L \frac{\overline{\sigma_E^2}}{\Delta E^2} &= \left(\frac{4 \left[1 + 2|\mu|^2 (1 + 2r \cos \varphi + r^2) \right]}{1 + 2\sigma_v^2 |\beta_1|^2 \left[1 + 2|\mu|^2 (1 + 2r \cos \varphi + r^2) \right] + \sqrt{1 + 2\sigma_v^2 |\beta_1|^2 \left[1 + 2|\mu|^2 (1 + 2r \cos \varphi + r^2) \right]}} \right) \times \\ &\times \frac{\left\{ 1 + 3|\beta_1|^2 \sigma_v^2 + 2|\mu|^2 \left[1 + 6|\beta_1|^2 \sigma_v^2 (1 + r \cos \varphi) \right] \right\}}{\left[1 + 2|\mu|^2 (1 + r \cos \varphi) \right]^2} = \mathcal{R}_E \end{aligned} \quad (127)$$

where $r := \frac{\alpha_1}{|\beta_1|}$ and $\cos \varphi := \text{Re} \left(\frac{\beta_1}{|\beta_1|} \Delta \right)$. In order to make it human-readable, we write

$$\begin{aligned} A &\equiv 1 + 2r \cos \varphi + r^2 = (1 + re^{i\varphi}) (1 + re^{-i\varphi}) \\ B &\equiv 1 + r \cos \varphi \\ X &\equiv 2\sigma_v^2 |\beta_1|^2 \\ Y &\equiv 1 + 2|\mu|^2 A \end{aligned} \quad (128)$$

and find

$$\mathcal{R}_E = \frac{4Y}{1 + XY + \sqrt{1 + XY}} \times \frac{1 + \frac{3}{2}X + 2|\mu|^2 [1 + 3XB]}{\left[1 + 2|\mu|^2 B \right]^2}. \quad (129)$$

The first factor behaves as $\approx 2Y$ for $X \ll 1$ and $\approx \frac{4Y}{XY} = \frac{4}{X}$ for $X \gg 1$. The second factor is asymptotically decreasing for large $|\mu|^2$, but for any fixed value, a strictly positive bound can be found.

References

- [1] Erik Torrontegui, Sabrina Ibáñez, Sofia Martínez-Garaot, Michele Modugno, Adolfo del Campo, David Guéry-Odelin, Andreas Ruschhaupt, Xi Chen, and Juan Gonzalo Muga. Shortcuts to adiabaticity. *Advances in Atomic, Molecular, and Optical Physics*, 62:117–169, 2013.
- [2] David Guéry-Odelin, Andreas Ruschhaupt, Adam Kiely, Erik Torrontegui, Sofia Martínez-Garaot, and Juan Gonzalo Muga. Shortcuts to adiabaticity: Concepts, methods, and applications. *Reviews of Modern Physics*, 91:045001, 2019.

- [3] Don N. Page and William K. Wootters. Evolution without evolution: Dynamics described by stationary observables. *Physical Review D*, 27:2885–2892, 1983.
- [4] Rodolfo Gambini and Jorge Pullin. The montevideo interpretation: How the inclusion of a quantum gravitational notion of time solves the measurement problem. *Universe*, 2020; 6(12)(236), 2020.
- [5] Esteban Calzetta. Not quite free shortcuts to adiabaticity. *Physical Review A*, 98(3):032107, 2018.
- [6] Richard P. Feynman and Frank L. Vernon. The theory of a general quantum system interacting with a linear dissipative system. *Annals of Physics*, 24:118–173, 1963.
- [7] Richard P. Feynman and Albert R. Hibbs. *Quantum Mechanics and Path Integrals*. McGraw-Hill College, 1965.
- [8] A. N. Pearson, Y. Guryanova, P. Erker, Edward Laird, G. Andrew D. Briggs, M. Huber, and N. Ares. Measuring the thermodynamic cost of timekeeping. *Physical Review X*, 11(2):021029, 2021.
- [9] Tan Van Vu and Keiji Saito. Time-cost-error trade-off relation in thermodynamics: The third law and beyond. *Phys. Rev. X*, 15:041029, Nov 2025.
- [10] S. J. van Enk and H. J. Kimble. On the classical character of control fields in quantum information processing. *Quantum Information & Computation*, 2(1):1–14, 2002.
- [11] Julio Gea-Banacloche. Some implications of the quantum nature of laser fields for quantum computations. *Phys. Rev. A*, 65:022308, 2002.
- [12] Andrew Silberfarb and Ivan H. Deutsch. Entanglement generated between a single atom and a laser pulse. *Phys. Rev. A*, 69:042308, 2004.
- [13] Ching-Kit Chan and L. J. Sham. Precision of electromagnetic control of a quantum system. *Physical Review A*, 84:032116, 2011.
- [14] Julio Gea-Banacloche and Mayo Miller. Quantum logic with quantized control fields beyond the $1/\bar{n}$ limit: Mathematically possible, physically unlikely. *Physical Review A*, 78:032331, 2008.
- [15] G. J. Milburn. Decoherence and the conditions for the classical control of quantum systems. *Philosophical Transactions of the Royal Society A*, 370:4469–4486, 2012.
- [16] Jake Xuereb, Florian Meier, Paul Erker, Mark T. Mitchison, and Marcus Huber. The impact of imperfect timekeeping on quantum control. *Phys. Rev. Lett.*, 131:160204, 2023.
- [17] Izaak Neri. Thermodynamic cost of random-time protocols. *Phys. Rev. E*, 112:044114, 2025.
- [18] Artur S. L. Malabarba, Anthony J. Short, and Philipp Kammerlander. Clock-driven quantum thermal engines. *New J. Phys.*, 17:045027, 2015.
- [19] Lea Lautenbacher, Giovanni Spaventa, Dario Cilluffo, Susana F. Huelga, and Martin B. Plenio. Physically constrained quantum clock-driven dynamics. *New J. Phys.*, 27:114501, 2025.
- [20] Daniel Martínez-Tibaduiza, Luis Pires, and Carlos Farina. Time-dependent quantum harmonic oscillator: a continuous route from adiabatic to sudden changes. *Journal of Physics B: Atomic, Molecular and Optical Physics*, 54(20):205401, nov 2021.
- [21] Nicolás F. Del Grosso, Fernando C. Lombardo, Francisco D. Mazzitelli, and Paula I. Villar. Fast adiabatic control of an optomechanical cavity. *Entropy*, 25(1), 2023.
- [22] Esteban Calzetta and Bei Lok Hu. *Nonequilibrium Quantum Field Theory*. Cambridge University Press, 2008.

- [23] Xi Chen, A. Ruschhaupt, S. Schmidt, A. del Campo, D. Guéry-Odelin, and J. G. Muga. Fast optimal frictionless atom cooling in harmonic traps: Shortcut to adiabaticity. *Phys. Rev. Lett.*, 104:063002, Feb 2010.
- [24] Dionisis Stefanatos, Justin Ruths, and Jr-Shin Li. Frictionless atom cooling in harmonic traps: a time-optimal approach. *Phys. Rev. A*, 82:063422, 2010.
- [25] L. Parker. Particle creation in expanding universes. *Phys. Rev. Lett.*, 21:562–564, Aug 1968.
- [26] Leonard Parker. Quantized fields and particle creation in expanding universes. i. *Phys. Rev.*, 183:1057–1068, Jul 1969.
- [27] Sebastian Deffner and Steve Campbell. Trade-off between speed and cost in shortcuts to adiabaticity. *Phys. Rev. Lett.*, 118:100601, 2017.
- [28] Anonymous. Quantum time crystal clock and its performance. *Physical Review Letters*, January 2026.
- [29] Murat Danageozian, Mark M. Wilde, and Francesco Buscemi. Thermodynamic constraints on quantum information gain and error correction: A triple trade-off. *PRX Quantum*, 3:020318, 2022.
- [30] Patrick Pietzonka and Udo Seifert. Universal trade-off between power, efficiency, and constancy in steady-state heat engines. *Phys. Rev. Lett.*, 120:190602, May 2018.